The first term on the right of Eq. (4.33) is sometimes called the *spinning* contribution (Longcope *et al.*, 2007) since it quantifies the injection of helicity due to the spinning of each patch. A patch of either sign spinning in a counterclockwise sense ($\omega_i > 0$) will inject negative helicity. This is natural since this sense of spinning would create a left-handed twist ($Tw < 0$) in a flux tube anchored to it. One complete rotation, $\omega_i \Delta t = 2\pi$, will change the helicity by $\Delta H_R = -\Phi_i^2$. There have been many observations (Brown *et al.*, 2003, for example) of sunspots spinning at rates as high as 3 degrees per hour ($\omega_i \sim 2 \times 10^{-3}$ rad/s); this motion adds helicity to the active region corona above it.

The second term on the right of Eq. (4.33), the *braiding helicity flux*, quantifies the helicity change occurring as patches move around one another. An opposing pair moving around one another in a clockwise sense ($d\theta_{ij}/dt > 0$) will inject positive helicity. If each has equal flux and spins at the same rate and sense at which they rotate then their spinning and braiding contributions will cancel. The cancellation makes sense, because a flux tube connecting the patches would be subject to nothing more than rigid rotation. That does not change the internal geometry of the field and thus should not change the helicity. Therefore, in order to inject helicity, the two patches must spin and rotate differently. The full braiding term in Eq. (4.33) actually includes a much wider range of contributions, including contributions from the relative motion of like-signed sources. In the end it does, however, quantify the helicity change arising from the restricted range of motions considered.

5

Magnetic reconnection

TERRY G. FORBES

5.1 Preamble

The widespread interest in reconnection results from the fact that it is a fundamental process that occurs in magnetized plasmas whenever the connectivity of the field lines changes in time. Reconnection is most commonly associated with geomagnetic and solar activity because such changes in field line connectivity can be directly observed, but there are many other, less well-known, applications ranging from meteorites and comet tails to accretion disks and galactic jets. Reconnection is also found in laboratory devices that have been built to study the feasibility of controlled thermonuclear reactors, as well as in several experiments that have been specifically designed to study reconnection as a basic plasma process. Those aspects of magnetic reconnection that depend primarily on the topology of the magnetic field tend to be of universal application. However, aspects that depend on the detailed characteristics of the plasma itself, such as its temperature and density, tend to be restricted to the specific application where such characteristics occur. Thus, there is no universal theory that can be applied to all situations.

5.2 Basic concepts

The term *magnetic reconnection* was introduced by Dungey (1953a), who was interested in the problem of particle acceleration in the Earth's magnetosphere. Earlier studies (Giovanelli, 1946; Hoyle, 1949) had considered the acceleration of particles at magnetic neutral points in the presence of an electric field produced by plasma convection, but these studies did not include the magnetic field produced by the current associated with the motion of the particle. Using the framework of non-ideal magnetohydrodynamics (MHD), Dungey argued that this current would take the form of a thin sheet in which the diffusion of the magnetic field would necessarily dominate. Furthermore, this diffusion would cause field lines passing

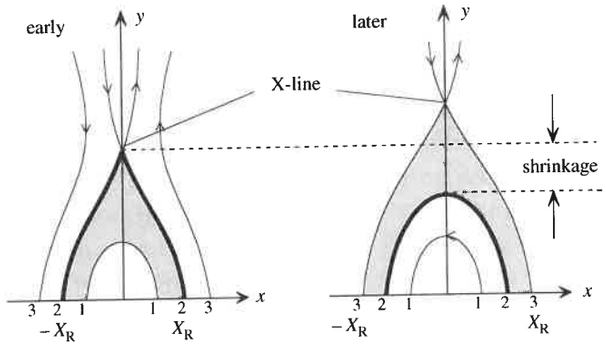

Fig. 5.1. The magnetic field line topology in the reconnection model of flare loops at two different times. The shaded area is the X-ray loop system, while the numbers at the base mark the footpoints of individual field lines. The outermost edges of the flare ribbons are located at X_R and $-X_R$.

through the current sheet to change their connectivity to one another. This process was described as field line "disconnection" followed by "reconnection".

5.2.1 Definitions

Magnetic reconnection can be defined quite generally as a change in the connectivity of field lines in time. This definition is based on the supposition that field lines can be uniquely identified and tracked in time. In an ideal plasma, i.e. one which satisfies the frozen-flux condition (see Section 3.2.3, the motion of an individual field line can be defined as being identical to the plasma motion in the direction perpendicular to the magnetic field. However, reconnection necessarily requires field lines to violate the frozen-flux condition so that they can change their connectivity, and when this happens it is not always possible to define the velocity or connectivity of a field line uniquely (Priest *et al.*, 2003). A tokomak plasma is an example of where problems can occur, although even here one can still talk about reconnection provided that there are well-organized flux surfaces. Generally reconnection is well defined in three dimensions if all the field lines map to surfaces, or localized regions, where the frozen-flux condition holds, because the connectivity of the field lines at any point in time can be uniquely established. Although it is possible to define a generalized reconnection process that does not require an X-type field line topology (see Section 5.3 below), all known applications to date do involve such a topology.

Before considering the full complications of reconnection in three dimensions, let us start by considering reconnection in two dimensions. Figure 5.1 shows a simple configuration derived from the standard two-dimensional model of a flare-loop

system. The magnetic field is shown at two different times. The panel on the left shows a time after the flare has occurred when the field is starting to relax. The panel on the right shows a later time. In each panel the horizontal line at the bottom corresponds to the solar surface. In the model it is assumed that the surface can be represented by an infinitely conducting and stationary plate. The feet of all the field lines are anchored (i.e. frozen) to this plate, so that a field line mapping to a given point on the surface maintains its identity for all times. As the field lines relax, they move toward the X-line in matched pairs and undergo reconnection. This reconnection process causes the region of closed field lines to grow with time. Newly closed field lines have a cusp shape while field lines lower down have a rounded shape, and the newly closed field lines pull away from the X-line as it moves upwards. This downward motion is usually referred to as "shrinkage" in the solar context, while in the Earth's geomagnetic tail it is referred to as "dipolarization". In the solar model the outermost edge of the flare-loop system lies along the field lines connecting the surface to the X-line. These lines constitute a separatrix as defined in the previous chapter, and in the model the footpoints of the separatrix correspond to the outer edge of the flare ribbons.

The field lines that have not yet reconnected can be described as "open" field lines, meaning that they extend upwards to infinity or to at least a very large distance. The field lines forming the loops below the X-line are said to be closed, meaning that they have a finite length and have both feet attached to the surface. In Fig. 5.1 the rate of reconnection is just the rate at which magnetic flux is transferred from the open region to the closed region. Quantitatively, we can express the rate of change of this flux as

$$\Phi_B = \frac{\mathrm{d}}{\mathrm{d}t}\int_0^{y_0(t)} B_x(0, y)\mathrm{d}y = \frac{\mathrm{d}}{\mathrm{d}t}\int_0^{X_R(t)} B_y(x, 0)\mathrm{d}x \qquad (5.1)$$

where y_0 is the location of the X-line on the y-axis. The time rate of change of this flux can be related to the electric field using Faraday's law (Eq. 10.9). The final result can be expressed as

$$\frac{\mathrm{d}\Phi_B}{\mathrm{d}t} = E_0 - E(X_R, 0) \qquad (5.2)$$

where E_0 is the electric field at the X-line and $E(X_R, 0)$ is the convective electric field $\mathbf{v} \times \mathbf{B}$ at the surface, at the footpoint of the field line that maps to the X-line (the separatrix). For solar flares the electric field, $E(X_R, 0)$, is negligible compared with the electric field at the X-line, so the rate of reconnection is related very simply to the apparent motion of the footpoint of the separatrix:

$$E_0 = B_y(X_0, 0)\,\dot{X}_0. \qquad (5.3)$$

The electric field E_0 at the X-line prescribes the rate at which magnetic flux is transferred from the open to the closed region. Since the flux crossing the y-axis below the X-line is the same as the flux between $x = 0$ and the separatrix footpoint at X_0, the electric field can be expressed simply as the vector product of the normal magnetic field at the separatrix footpoint and the apparent velocity of the footpoint across the surface.

For reconnection in the Earth's magnetotail, $E(X_R, 0)$ is not negligible and its value must be measured to determine the reconnection rate. Such measurements can be made from the ground, using radar signals reflected off the ionosphere to determine the convective flow and the corresponding convective electric field (see Blanchard *et al.*, 1996).

5.2.2 MHD theory versus kinetic theory

Reconnection can occur in a broad range of environments. Some, such as the convection zone in the outer layer of the solar interior, are completely dominated by binary particle collisions. However, in many cases of interest the plasma is nearly collisionless, i.e. the mean free path for binary collisions between particles is much greater than the characteristic scale length of the system. The Earth's magnetosphere is a classic example of such a collisionless system. Because MHD does not explicitly treat individual particle motions, one may jump to the false conclusion that it is of little use in collisionless plasmas. In reality, MHD and its two-fluid variants usually describe the global behavior of collisionless plasmas very well. For example, beyond ten solar radii the solar wind is a completely collisionless plasma, yet MHD models describe its global velocity, temperature, and density quite well, including such time-dependent aspects as shock disturbances, stream interactions, and turbulence.

Thus ideal MHD, and even non-ideal MHD, can successfully describe the average bulk properties of collisionless plasmas. Ideal (dissipationless) MHD embodies conservation principles, such as mass, momentum, and energy conservation, which are universal for both collisional and collisionless systems (Parker, 1996). Resistive MHD, which assumes that dissipation is a local property of the plasma, can be valid if wave–particle or wave–wave interaction prevent long-range interactions in the plasma.

Despite the past successes of MHD in explaining the dynamics of collisionless plasmas, however, there is good reason to be cautious when applying it to reconnection. By definition, reconnection cannot occur in ideal MHD because it depends on the diffusion of field lines through the plasma, often in small-scale structures such as current sheets. In this situation kinetic theory is essential for calculating the effective resistivity.

To determine a realistic resistivity for a collisionless plasma requires consideration of the generalized Ohm's law. For a fully ionized plasma it can be written as

$$\mathbf{E} = -\mathbf{v} \times \mathbf{B} + \frac{\mathbf{j}}{\sigma} + \frac{m_e}{ne^2}\left[\frac{\partial \mathbf{j}}{\partial t} + \nabla \cdot (\mathbf{vj} + \mathbf{jv})\right] - \frac{\mathbf{j} \times \mathbf{B}}{ne} - \frac{\nabla \mathbf{p}_e}{ne}, \tag{5.4}$$

where $\mathbf{vj}$ and $\mathbf{jv}$ are dyadic tensors and $\mathbf{p}_e$ is the electron stress tensor (Rossi and Olbert, 1970). The first term on the right-hand side of this equation is the convective electric field, while the second term is the field associated with Ohmic dissipation caused by electron–ion collisions. The conductivity σ is the inverse of the electrical resistivity η_e. The next three terms describe the effects of electron inertia and the next to the last term expresses the Hall effect. Ion inertia can be considered negligible because the large mass of the ions means that they do not contribute significantly to a change in the current density. Finally, the last term includes the electron gyroviscosity, which is considered by many to be important at a magnetic null (Strauss, 1986; Dungey, 1994). For a partially ionized plasma, collisions between charged particles and neutrals lead to additional terms associated with ambipolar diffusion.

Although all the terms on the right-hand side of the generalized Ohm's law (5.4), other than the first, allow field lines to slip through the plasma, they do not all produce dissipation. For example, the inertial terms do not cause the entropy of the plasma to increase. Thus, even though one may speak of inertial effects as creating an effective resistivity, this resistivity does not necessarily lead to dissipation.

Which terms are important in a particular situation depends not only upon the plasma parameters but also upon the length and time scales for variations of these parameters (Elliott, 1993; Sturrock, 1994). For magnetic reconnection, we normally want to know which non-ideal terms are likely to be significant within the current sheet where the frozen-flux condition is violated. Since each non-ideal (i.e. diffusion) term in the generalized Ohm's law contains either a spatial or temporal gradient, we can estimate the significance of any particular term by computing the gradient scale length L_0 required to make the term as large as the value of the convective electric field $\mathbf{v} \times \mathbf{B}$ outside the diffusion region.

Consider, for example, the three inertial terms $[\partial \mathbf{j}/\partial t + \nabla \cdot (\mathbf{vj} + \mathbf{jv})]$ on the right-hand side of the generalized Ohm's law. If we assume that $\nabla \approx 1/L_0$, $|\mathbf{j}| \approx B_0/(\mu L_0)$, and $\partial/\partial t \approx V_0/L_0$, say, where L_0 is a typical length scale and V_0 a typical velocity, then these three terms will be of the same order as the convective electric field if

$$\frac{m_e}{ne^2}\frac{V_0 B_0}{\mu L_0^2} \approx V_0 B_0.$$

In other words, in order for the inertial terms to be important in a current sheet, its thickness $L_{\rm inertia}$ should be given by

$$L_{\rm inertia} \approx c\left(\frac{m_{\rm e}\epsilon_0}{ne^2}\right)^{1/2} \approx \lambda_{\rm e}, \tag{5.5}$$

where

$$\lambda_{\rm e} = \frac{c}{\omega_{\rm pe}} = \left(\frac{m_{\rm e}}{ne^2\mu}\right)^{1/2} = 5.30 \times 10^6\, n^{-1/2} \tag{5.6}$$

is the electron inertial length or skin depth, $c = (\epsilon_0\mu)^{1/2}$ is the speed of light, and $\omega_{\rm pe} = [(e^2 n_{\rm e})/(\epsilon_0 m_{\rm e})]^{1/2}$ is the electron plasma frequency.

Similarly, for the Hall term $\mathbf{j} \times \mathbf{B}/(ne)$,

$$\frac{B_0^2}{ne\mu L_0} \approx V_0 B_0$$

or

$$L_{\rm Hall} \approx \frac{c}{M_{\rm A}}\left(\frac{\tilde{\mu} m_{\rm p}\epsilon_0}{ne^2}\right)^{1/2} \approx \frac{\lambda_{\rm i}}{M_{\rm A}}, \tag{5.7}$$

where

$$\lambda_{\rm i} = \frac{c}{\omega_{\rm pi}} = \left(\frac{\tilde{\mu} m_{\rm p}}{ne^2\mu}\right)^{1/2} = 2.27 \times 10^8 \left(\frac{\tilde{\mu}}{n}\right)^{1/2} \tag{5.8}$$

is the ion inertial length or skin-depth. The Alfvén Mach number equals $M_{\rm A} = V_0/V_{\rm A} = V_0 B_0 (\mu\tilde{\mu} m_{\rm p} n)^{-1/2}$, with $\tilde{\mu} = \overline{m}/m_{\rm p}$ the mean atomic weight, $\omega_{\rm pi} = [(q_{\rm i}^2 n_{\rm i})/(\epsilon_0 m_{\rm i})]^{1/2}$ the ion plasma frequency, and $V_{\rm A}$ the Alfvén speed.

For the electron stress term $\nabla \mathbf{p}_{\rm e}/(ne)$ we can write

$$\frac{nk_{\rm B}T}{neL_0} \approx V_0 B_0$$

if we assume that $|\mathbf{p}_{\rm e}| \approx nk_{\rm B}T_{\rm e}$ and $T_{\rm e} \approx T_{\rm i} \approx T$. Solving for L_0 leads to

$$L_{\rm stress} \approx \frac{\beta^{1/2}}{M} R_{\rm gi}, \tag{5.9}$$

where

$$\beta = nk_{\rm B}T\left(\frac{2\mu}{B_0^2}\right) = 3.47 \times 10^{-29}\frac{nT}{B_0^2} \tag{5.10}$$

and

$$R_{\rm gi} = \frac{(k_{\rm B}T_{\rm i} m_{\rm p}\tilde{\mu})^{1/2}}{eB_0} = 9.49 \times 10^{-7}\frac{(T_{\rm i}\tilde{\mu})^{1/2}}{B_0} \tag{5.11}$$

are the plasma β-parameter and the ion gyroradius, respectively.

Finally, for the collision term $\mathbf{j}/\sigma$,

$$\frac{B_0}{\mu\sigma L_0} \approx M v_{\rm A} B_0,$$

where the product $(\mu\sigma)^{-1}$ is also the magnetic diffusivity η. Using Spitzer's formula for the collisional resistivity $\eta_{\rm e}$ of a plasma (see Eq. 3.19) we obtain

$$\eta_{\rm e} = \frac{1}{\sigma} = \frac{(k_{\rm B} m_{\rm e} T_{\rm e})^{1/2}}{ne^2\lambda_{\rm mfp}}, \tag{5.12}$$

where

$$\lambda_{\rm mfp} = 3(2\pi)^{3/2}\frac{(k_{\rm B}T_{\rm e}\epsilon_0)^2}{ne^4 \ln\Lambda} = 1.07 \times 10^9 \frac{T_{\rm e}^2}{n \ln\Lambda} \tag{5.13}$$

is the mean free path for electron–ion collisions (Schmidt, 1966). Combining these expressions with those for the electron and ion inertial lengths we obtain

$$L_{\rm collision} \approx \frac{\beta^{1/2}}{M}\frac{\lambda_{\rm e}\lambda_{\rm i}}{\lambda_{\rm mfp}}. \tag{5.14}$$

Note that the length scale $L_{\rm collision}$ of the spatial variations required to achieve significant field-line diffusion is inversely proportional to the mean free path $\lambda_{\rm mfp}$. As $\lambda_{\rm mfp}$ increases, the diffusion caused by collisions becomes less effective, and increasingly sharper gradients are required to maintain the size of the dissipation term $\mathbf{j}/\sigma$.

Tables 5.1 and 5.2 list various plasma parameters along with the characteristic scale lengths for four different regions where reconnection is thought to occur. The parameter $L_{\rm e}$ is the global (external) scale size of the region, and the fundamental quantities from which the other parameters are derived are the density n, temperature T, and magnetic field B. For convenience, we assume that the Alfvén Mach number $M_{\rm A}$ is unity and that the electron and ion temperatures are roughly equal. The most extreme plasma environments listed in Table 5.1 occur in the magnetosphere, which is completely collisionless, and in the solar interior, which is highly collisional.

In addition to the parameters discussed above, Table 5.1 also lists the value of the *Debye length*

$$\lambda_{\rm D} = \left(\frac{\epsilon_0 k_{\rm B} T_{\rm e}}{ne^2}\right)^{1/2} = 69.0\left(\frac{T_{\rm e}}{n}\right)^{1/2}. \tag{5.15}$$

The number of particles within a Debye sphere (i.e. $4\pi n\lambda_{\rm D}^3/3$) must be larger than unity in order for the generalized Ohm's law to hold. Otherwise, the collective behavior which characterizes a plasma breaks down. The number of particles in a

Table 5.1. *Comparison of plasma parameters in different environments (in MKS units, i.e. length scales in* m, *n in* m^{-3}, *T in* K, *B in tesla, electric fields in* $V\,m^{-1}$)

Parameter	Laboratory experiments[a]	Terrestrial magnetosphere[b]	Solar corona[c]	Solar interior[d]
L_e	10^{-1}	10^{7}	10^{8}	10^{7}
n	10^{20}	10^{5}	10^{15}	10^{29}
T	10^{5}	10^{7}	10^{6}	10^{6}
B	10^{-1}	10^{-8}	10^{-2}	10^{1}
λ_D	10^{-6}	10^{3}	10^{-3}	10^{-10}
R_{gi}	10^{-3}	10^{5}	10^{-1}	10^{-4}
λ_i	10^{-2}	10^{6}	10^{1}	10^{-6}
$\ln \Lambda$	11	33	19	3
λ_{mfp}	10^{-2}	10^{16}	10^{4}	10^{-9}
β	10^{-2}	10^{-1}	10^{-4}	10^{4}
$L_u\ (\approx R_m)$	10^{3}	10^{14}	10^{14}	10^{10}
E_D	10^{3}	10^{-13}	10^{-2}	10^{11}
$E_A\ (= v_A B)$	10^{4}	10^{-2}	10^{5}	10^{4}
$E_{SP}\ (= E_A/\sqrt{R_{me}})$	10^{2}	10^{-9}	10^{-3}	10^{-2}

[a] MRX at Princeton Plasma Physics Laboratory.
[b] Plasma sheet.
[c] Above a solar active region.
[d] Base of the solar convection zone.

Table 5.2. *Diffusion lengths (in meters) from the generalized Ohm's law*

Characteristic length	Laboratory experiments[a]	Terrestrial magnetosphere[b]	Solar corona[c]	Solar interior[d]
$L_{inertia}(\lambda_e)$	10^{-4}	10^{4}	10^{-1}	10^{-8}
$L_{Hall}(\lambda_i)$	10^{-2}	10^{6}	10^{1}	10^{-6}
L_{stress}	10^{-3}	10^{5}	10^{-3}	10^{-2}
$L_{collision}$	10^{-4}	10^{-7}	10^{-7}	10^{-3}

[a] MRX at Princeton Plasma Physics Laboratory.
[b] Plasma sheet.
[c] Above a solar active region.
[d] Base of the solar convection zone.

Debye sphere for the environments shown in Table 5.1 ranges from 10^{14} for the magnetosphere to only about four for the solar interior at the base of the convection zone. Also shown in the table is the Lundquist number L_u, which is the same as the magnetic Reynolds number R_m when the flow and Alfvén speeds are the same. For a collisional plasma, the Lundquist number based on L_e can be expressed as

$$L_u = \frac{L_e v_A}{\eta} = \frac{L_e T_e^{3/2} B_0}{(\tilde{\mu} n)^{1/2} \ln \Lambda} 2.07 \times 10^8. \tag{5.16}$$

Here η is the magnetic diffusivity, which is defined as $1/(\mu\sigma) = \eta_e/\mu$, where σ is the conductivity and η_e is the electrical resistivity. In the expression on the far right, η has been replaced by Spitzer's formula for the electrical resistivity of a collisional plasma (Priest and Forbes, 2000).

The characteristic scale lengths in Table 5.1 provide an indication of which terms in the generalized Ohm's law are likely to be important for the reconnection of current sheets. As with MHD shocks and turbulence, the large-scale dynamics of the flow causes the current sheet to thin until it reaches a length scale where field line diffusion is effective. Thus, in principle, the term with the largest characteristic length scale in Table 5.2 is the one that will be most important. Since the Hall term has the largest length in every environment except the solar interior, one might conclude that it is generally the most important. However, this conclusion does not take into consideration the fact that the Hall term tends to zero in the region of a magnetic null point or sheet. The Hall term on its own does not contribute directly to reconnection, since it freezes the magnetic field to the electron flow. To know whether a particular term is really as important as is suggested by its relative length scale requires a complete analysis of the kinetic dynamics, which is a rather formidable task. An excessively small length scale, however, does indicate that any process associated with that term is unlikely to be important. Therefore, on this basis we can conclude that collisional diffusion is not important in the terrestrial magnetosphere or the solar corona and that the electron inertial terms and the Hall term are not important in the solar interior.

Although the collision length scale $L_{collision}$ is equally small in both the magnetosphere and the corona, the general importance of the collisions in these two regions is quite different. In the magnetosphere the collision mean free path λ_{mfp} is nine orders of magnitude larger than the global scale size L, but in the corona it is four orders of magnitude smaller than the global scale. Thus, we can be confident that collisional transport theory applies to large-scale structures in the corona even though it is not applicable within thin current sheets or dissipation layers. By contrast, in the magnetosphere collisions are so few that collisional transport theory does not apply at any scale.

Another important issue concerning the applicability of collisional theory is the strength of the electric field, in a frame moving with the plasma. If this field exceeds

the *Dreicer electric field*, defined by

$$E_{\mathrm{D}} = \frac{e \ln \Lambda}{4\pi \epsilon_0 \lambda_{\mathrm{D}}^2} = \frac{e^3 \ln \Lambda\, n}{4\pi \epsilon_0^2 k_{\mathrm{B}} T_{\mathrm{e}}} = 3.02 \times 10^{-13} \frac{n \ln \Lambda}{T_{\mathrm{e}}}, \tag{5.17}$$

runaway acceleration of electrons will occur. The most likely location for the production of runaway electrons in a reconnection process is in a thin current sheet that forms at the null point. This field could be as large as the convective electric field based on the Alfvén speed, that is

$$E_{\mathrm{A}} = v_{\mathrm{A}} B_0 = 2.18 \times 10^{16} \frac{B_0^2}{(\tilde{\mu} n)^{1/2}},$$

or as low as the Sweet–Parker electric field

$$E_{\mathrm{SP}} = \frac{E_{\mathrm{A}}}{R_{\mathrm{m}}^{1/2}},$$

where R_{m} is the magnetic Reynolds number based on the inflow Alfvén speed (i.e. the inflow Lundquist number). As shown in Table 5.1, the Dreicer field in the magnetosphere is much smaller than E_{A} or E_{SP}, so runaway electrons will always be generated by reconnection there. However, in the solar interior the Dreicer field is so large that the runaway acceleration of electrons never occurs. In the intermediate regimes of the laboratory and the solar corona the Dreicer field lies between E_{A} and E_{SP}, so perhaps runaway electrons are only produced when very fast reconnection occurs.

Even in completely collisionless environments such as the Earth's magnetosphere, it is still sometimes possible to express the relation between electric field and current density in terms of an anomalous resistivity. For example, Lyons and Speiser (1985) showed that the electron inertial terms in the generalized Ohm's law lead to an anomalous resistivity

$$\frac{1}{\sigma^*} = \frac{\pi B_z}{2ne},$$

where B_z is the field normal to the current sheet. This resistivity is derived solely from a consideration of the particle orbits, and in the magnetotail current sheet it may be larger than any anomalous resistivity due to wave–particle interactions. A typical example of the latter is the anomalous resistivity due to ion acoustic waves (Priest, 1982; Benz, 1993).

5.3 Reconnection in two dimensions

In this section we outline basic two-dimensional approaches to magnetic reconnection, using on resistive MHD theory. More detailed information can be found in the original papers and in recent books by Biskamp (2000) and Priest and Forbes (2000).

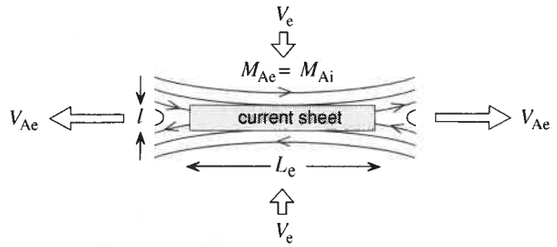

Fig. 5.2. The Sweet–Parker field configuration. Plasma (open arrows) flows into the upper and lower sides of a current sheet of length L_{e} but must exit through the narrow tips of the sheet, of width l. Because the field is assumed to be uniform in the inflow region, the external Alfvén Mach number $M_{\mathrm{Ae}} = v_{\mathrm{e}}/v_{\mathrm{Ae}}$ at a large distance is the same as the internal Alfvén Mach number M_{Ai} at the midpoint edge of the current sheet.

5.3.1 Steady-state models

A few years after Dungey's introduction of the concept of reconnection, Sweet (1958) and Parker (1957) developed the first quantitative model. In order to make the analysis as analytically tractable as possible, they focused on the problem of two-dimensional steady-state reconnection in an incompressible plasma. They assumed that reconnection occurs in a current sheet whose length is set by the global scale L_{e} of the field, as shown in Fig. 5.2. Under these conditions they determined that the speed of the plasma flowing into the current sheet is approximately

$$v_{\mathrm{e}} = v_{\mathrm{Ae}} L_{\mathrm{u}}^{-1/2} \tag{5.18}$$

where $L_{\mathrm{u}} = \mu_0 L_{\mathrm{e}} v_{\mathrm{Ae}}/\eta$ is the Lundquist number and η is the magnetic diffusivity. The global scale length is L_{e}, and $v_{\mathrm{Ae}} = B_{\mathrm{e}}/\sqrt{\mu_0 \rho_{\mathrm{e}}}$ is the Alfvén speed in the inflow region. Sometimes L_{u} is referred to as the magnetic Reynolds number, although the latter term is normally used for a similar number based on a typical flow speed rather than the Alfvén speed. The outflow speed of the plasma from the current sheet is V_{Ae} and does not depend on the value of L_{u}. The reconnection rate in two dimensions is measured by the electric field at the reconnection site. This electric field is perpendicular to the plane of Fig. 5.2 and prescribes the rate at which magnetic flux is transported from one topological domain to another. In two-dimensional (2D) steady-state models this electric field is uniform in space. Therefore the Alfvén Mach number, $M_{\mathrm{Ae}} = v_{\mathrm{e}}/v_{\mathrm{Ae}}$, provides a quantitative measure of the reconnection

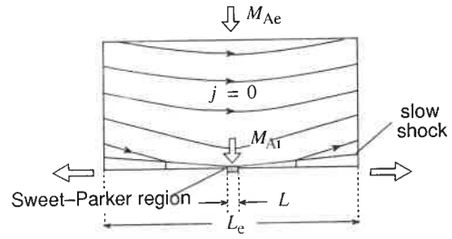

Fig. 5.3. Petschek's field configuration. Here the length L of the Sweet–Parker current sheet is much shorter than the global scale length L_e, and the magnetic field in the inflow is non-uniform. Two pairs of standing slow-mode shocks extend outwards from the central current sheet. Petschek's model assumes that the current density in the inflow region is zero and that there are no external sources of field at large distance.

rate relative to the characteristic electric field $v_{Ae}B_e$. In terms of this number, the Sweet–Parker reconnection rate is just $M_{Ae} = {L_u}^{-1/2}$.

In astrophysical and space plasmas L_u is very large ($L_u \gg 10^6$), so Sweet–Parker reconnection is usually too slow to account for phenomena such as geomagnetic substorms or solar flares. Petschek (1964) proposed a model with an increased rate of reconnection resulting from the use of a current-sheet length greatly reduced from that of the Sweet–Parker model. He did this by encasing their current sheet, in an exterior field with global scale length L_e. He also introduced two pairs of standing slow-mode shocks radiating outwards from the tip of the current sheet, as shown in Fig. 5.3. In Petschek's solution most of the energy conversion comes from these shocks, which accelerate and heat the plasma to form two hot outflow jets.

Petschek also assumed that the magnetic field in the inflow region was current-free and that there were no sources of field at large distances. These assumptions, together with the trapezoidal shape of the inflow region created by the slow shocks, lead to a logarithmic decrease in the magnetic field as the inflowing plasma approaches the Sweet–Parker current sheet. This variation in the field leads in turn to Petschek's formula for the maximum reconnection rate, namely

$$M_{Ae[Max]} = \pi/(8 \ln L_u) \tag{5.19}$$

where L_u is again the Lundquist number and M_{Ae} is the Alfvén Mach number in the region far upstream of the current sheet, as shown in Fig. 5.3. Because of its logarithmic dependence on L_u, the Petschek reconnection rate is many orders of magnitude greater than the Sweet–Parker rate, and for most space and laboratory applications Petschek's formula predicts that $M_{Ae} \approx 10^{-1}$ to 10^{-2}.

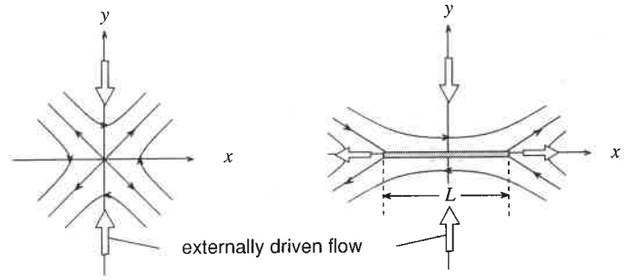

Fig. 5.4. Syrovatskii's field configuration. Unlike Petschek's configuration, this has external sources which produce an X-type configuration even when local sources of current are absent. The application of external driving to an X-type configuration (left-hand panel) creates a current sheet (right-hand panel) whose length L depends on the temporal history of the driving and the rate at which reconnection operates. The fastest reconnection rate occurs when L is equal to the external scale length L_e.

Petschek's model uses the Sweet–Parker model to describe the flow of plasma and fields in the diffusion region. Because the Sweet–Parker model only gives average properties for this region, such as its length and thickness, no detailed matching is possible between the flows in the diffusion region and the flows in the external region outside. This lack of detailed matching is sometimes misunderstood to mean that there is no matching at all (Biskamp, 2000), but in fact the average properties of the diffusion region are rigorously matched to the external region to the extent that the Sweet–Parker model allows (Vasyliūnas, 1975b).

It is not always appreciated that Petschek's reconnection model is a particular solution of the MHD equations which applies only when special conditions are met. First, it requires that the flows into the reconnection region arise spontaneously without external forcing (Forbes, 2001). In general, driving the plasma externally creates a significant current density in the inflow region, and this violates Petschek's assumption that the inflow field is approximately potential. Second, Petschek's solution also requires that there be no external source of field in the inflow region. In other words, the field in question must be just the field produced by the currents in the diffusion region and the slow shocks. In many applications of interest neither of these conditions is met.

An alternative approach to reconnection in current sheets was pioneered by Green (1965) and Syrovatskii (1971), who considered what happens when a weak flow impinges on an X-line in a strongly magnetized plasma, as indicated in Fig. 5.4. The imposed flow creates a current sheet which achieves a steady state when the rate of field line diffusion through the sheet matches the speed of the flow. A quantitative model of this process was published by Somov (1992).

For a steady-state MHD model the spatial variation of the field in the inflow region is the key quantity which determines how the reconnection rate scales with the Lundquist number L_u. For any such model, the electric field is uniform and perpendicular to the plane of the field. Thus outside the diffusion region we have $E_o = -v_y B_x$, where E_o is a constant, v_y is the inflow along the axis of symmetry (the y-axis in Fig. 5.4), and B_x is the corresponding field. Thus the inflow Alfvén Mach number, M_{Ae}, at large distances can be expressed as

$$M_{Ae} = M_{Ai} B_i^2 / B_e^2 \tag{5.20}$$

where M_{Ai} is the Alfvén Mach number at the current sheet, B_i is the magnetic field at the edge of the current sheet, and B_e is the magnetic field at a large distance.

In Syrovatskii's model the field along the inflow axis of symmetry is

$$B_x = B_i(1 + y^2/L^2)^{1/2} \tag{5.21}$$

where B_i is the field at the current sheet, y is the coordinate along the inflow axis, and L is the length of the current sheet. Combining (5.21) with (5.20) yields

$$M_{Ae} = M_{Ai} \frac{1}{1 + L_e^2/L^2}, \tag{5.22}$$

which has its maximum value when $L = L_e$. Thus the maximum reconnection rate in Syrovatskii's model scales as $L_u{}^{-1/2}$, the same as for the Sweet–Parker model.

By comparison, the field in Petschek's model along the inflow axis varies approximately as

$$B_x = B_i \frac{1 - (4/\pi) M_{Ae} \ln(L_e/y)}{1 - (4/\pi) M_{Ae} \ln(L_e/l)} \tag{5.23}$$

where l is the current sheet thickness. (This expression for the field is only a rough estimate; the actual variation in the region $y < L$ (Vasyliūnas, 1975b; Priest and Forbes, 2000) is more complex.) Evaluating B_x at $y = L_e$ and substituting the result into Eq. (5.20) gives

$$M_{Ai} = M_{Ae}[1 - (4/\pi) M_{Ae} \ln(L_e/l)]^{-2}. \tag{5.24}$$

The Sweet–Parker theory can be used to eliminate L_e/l, so as to obtain an expression for M_{Ae} as a function of L_u. This expression has a maximum value, given by Eq. (5.19).

The spatial variation in the field in the inflow region is given for the Syrovatskii and the Petschek models in Fig. 5.5. Although both fields increase with distance away from the current sheet, the rate at which they increase is markedly different. At large distances the rate of increase in the Syrovatskii model is dominated by the external field, whose variation is fixed and independent of the reconnection rate. By contrast, the variation in the Petschek model is closely coupled to the reconnection

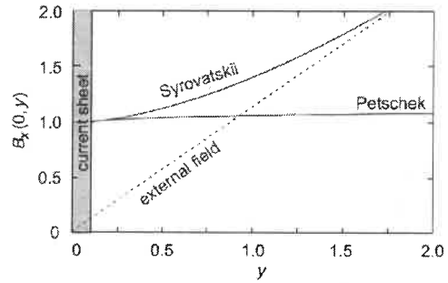

Fig. 5.5. The variation in the magnetic field, in the inflow region of Petschek's and Syrovatskii's models, along the axis of symmetry (the y-axis). At large distances the variation in Syrovatskii's model is determined by external field sources at infinity. The magnetic fields are normalized to their values at the edge of the current sheet, and the distance y is normalized to the length L of the current sheet. For the Petschek curve, $M_{Ae} = 0.02$, $l = 0.1L$, and $L_e = 2L$.

rate, disappearing altogether when the rate goes to zero. This is one of the main reasons why the two models give such different predictions for the reconnection rate. It also explains why the numerical simulation by Biskamp (1986) of the evolution shown in Fig. 5.4 produces a Sweet–Parker rather than a Petschek-type scaling.

Even in circumstances where Petschek's model would be expected to apply it apparently does not. Several numerical simulations (Biskamp, 1986; Scholer, 1989) were carried out in an attempt to verify the steady-state solution found by Petschek (1964), but none of these simulations has been able to replicate the scaling results that are predicted by Petschek's solution if the resistivity is kept uniform and constant. Only when a non-uniform, localized, resistivity model (Ugai, 1988; Yan *et al.*, 1992) is used does the Petschek configuration appear. The fact that the resistivity apparently needs to be non-uniform does not contradict Petschek's model because the model makes no explicit assumption about whether the resistivity is uniform or not. It is equally valid for both cases because it assumes only that the region where resistivity is important is localized. The numerical experiments carried out to date imply that the diffusion region can be localized only by enhancing the resistivity near the X-line. Whether there might be other ways to localize the diffusion region (e.g. assuming a non-uniform viscosity) remains unknown.

Although Petschek assumed that the current density j in the inflow region was zero to first order, it is not actually necessary to make such an assumption to obtain a solution. More generally, j can be non-zero to first order in the expansion of the inflow equations, so that the inflow magnetic field is no longer determined by solving Laplace's equation ($\nabla^2 A = 0$) for the vector potential A but by solving Poisson's equation ($\nabla^2 A = -\mu_0 j$) instead (Priest and Forbes, 1986). The relaxation of the assumption that j is zero introduces an additional degree of freedom,

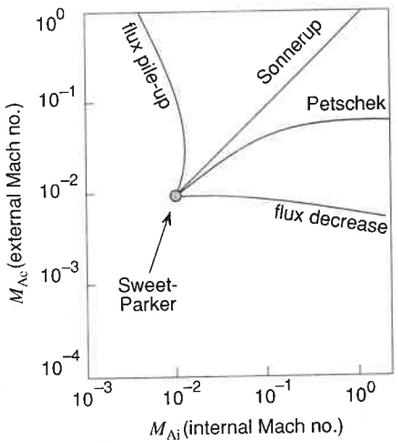

Fig. 5.6. External Alfvén Mach number M_{Ae} vs. the internal Alfvén Mach number M_{Ai}, for the family of solutions obtained by Priest and Forbes (1986). These solutions were obtained by an expansion in terms of the inflow Alfvén Mach number for small variations of the field around the uniform inflow field assumed in the Sweet–Parker model. Solutions with the labeled characteristics are obtained for different choices of the parameters describing the distant boundary conditions.

so that there is now a family of solutions (Fig. 5.6). These solutions can be summarized in terms of the relation between M_{Ai}, the internal Alfvén Mach number at the entrance to the diffusion region, and M_{Ae}, the Alfvén Mach number at the exterior inflow boundary (Fig. 5.3). The relation is

$$\frac{{M_{Ae}}^{1/2}}{{M_{Ai}}^{1/2}} = 1 - \frac{4}{\pi} M_{Ae}(1-b)\left[0.834 - \ln\tan\left(\frac{\pi}{4} {L_u}^{-1} M_{Ae}^{-1/2} M_{Ai}^{-3/2}\right)\right] \tag{5.25}$$

where b is a parameter whose value corresponds to the assumptions made about the inflow boundary conditions at $y = L_e$. The relation (5.25) is plotted in Fig. 5.6 for $S = 100$ for various values of b. When $b = 0$ Petschek's solution is obtained, and when $b = 1$ a solution equivalent to that of Sonnerup (1970) is obtained. When $b < 1$, the solution somewhat resembles Syrovatskii's solution in that the magnetic field increases markedly with distance away from the current sheet. For these solutions the maximum reconnection rate is the same as for the Sweet–Parker model.

As b increases beyond unity, a flux-pile-up regime occurs where the magnetic field increases as the diffusion region current sheet is approached (Fig. 5.7). For a very strong flux pile-up with $b \gg 1$, the flow approaches the MHD stagnation-point-flow solution found by Parker (1973) and Sonnerup and Priest (1975). The stagnation-point flow appears to be very fast since formally there is no limit to

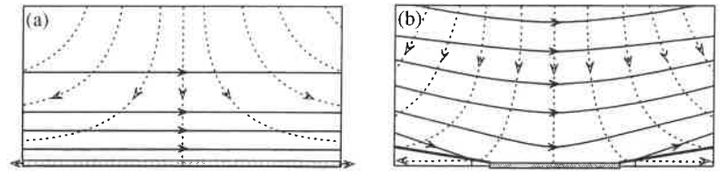

Fig. 5.7. (a) The stagnation-point-flow solution obtained by Parker (1973) for magnetic field annihilation at a current sheet, and (b) the closely related flux-pile-up solution obtained by Priest and Forbes (1986).

the value of M_{Ae}. However, large values of M_{Ae} require large variations in the gas pressure, which are not possible unless the plasma β is very much greater than unity. For low-β plasmas the amount of pile-up is limited, and when this limitation is taken into consideration the reconnection rate is found to scale at the relatively slow Sweet–Parker rate (Litvinenko *et al.*, 1996; Priest, 1996; Litvinenko and Craig, 1999). For a low-β plasma the fastest rate occurs for $b = 0$, which is Petschek's solution.

Vasyliūnas (1975b) was the first to point out that the differences between reconnection solutions are often related to the behavior of the gas and magnetic pressures in the inflow region. The inflow can be characterized as undergoing a compression or an expansion depending on whether the gas pressure increases or decreases as the plasma flows in towards the X-point. These compressions or expansions can be characterized further as being of the fast-mode type or the slow-mode type, depending on whether the magnetic pressure changes in the same sense as the gas pressure (fast-mode type) or in the opposite sense (slow-mode type). For the family of solutions above one finds that in Petschek's solution ($b = 0$) the gas pressure is uniform to second order in the expansion parameter M_{Ae} so that, to this order, the plasma is neither compressed nor rarefied as it flows towards the X-point. For solutions with $b < 0$ the plasma undergoes a slow-mode compression, while for $b > 1$ it undergoes a slow-mode expansion. Between $b = 0$ and $b = 1$ the solutions have a hybrid character; slow-mode and fast-mode expansions exist in different regions of the inflow. It is also possible to have hybrid solutions in which slow-mode expansions and slow-mode compressions co-exist in different regions of the inflow (Strachan and Priest, 1994), although this does not happen for the above family of solutions.

5.3.2 *Two-dimensional time-dependent reconnection*

So far, we have only considered the development of steady-state models of reconnection. However, for many phenomena (such as flares and geomagnetic substorms)

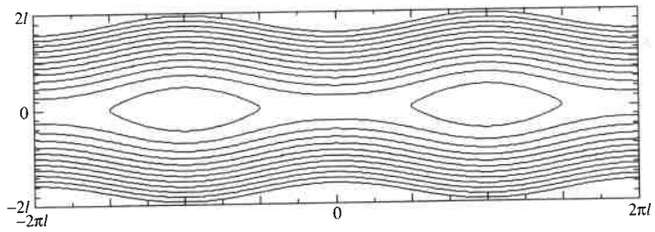

Fig. 5.8. Typical magnetic island structure resulting from the tearing instability of a plane current sheet. The contour lines show magnetic flux surfaces of the magnetic field (Forbes, 2006).

reconnection occurs on such short time scales that a steady or quasi-steady state does not exist. For example, in high-speed coronal mass ejections (with velocities greater than about 1000 km/s) the current sheet created by the ejection grows in length at a speed which is of the order of, or in excess of, the ambient Alfvén wave speed (Lin and Forbes, 2000). Steady-state reconnection is primarily confined to situations where the external field and the flows vary slowly compared with the characteristic Alfvén time scale of the system.

Time-dependent reconnection was first considered by Dungey (1958), who noted that motions in the vicinity of an X-line in a strongly magnetized plasma can lead to the very rapid formation of a current sheet. The first explicit solution demonstrating this possibility was published by Imshennik and Syrovatskii (1967). They found that if the gas pressure is negligible and the resistivity is small then, during the initial formation of the sheet, the electric field E at the X-line grows at a rate proportional to $(t_c - t)^{4/3}$ where t_c is about twice the Alfvén time scale of the system. At the time t_c the electric field becomes infinite, but the assumptions underlying the solution break down before this time is reached. Although there have been several analyses and extensions of this solution (Priest and Forbes, 2000), little effort has been made to apply this theory to highly dynamic phenomena such as flares.

Most theoretical effort on time-dependent reconnection has concentrated on the *tearing instability* (Furth *et al.*, 1963), illustrated in Fig. 5.8. This is a non-ideal instability in which the magnetic reconnection of field lines plays a central role. Tearing has been invoked in some flare models as a mechanism for releasing magnetic energy (Heyvaerts *et al.*, 1977) but, considered as a possible flare mechanism, it suffers from the fact that resistive tearing is relatively slow (Steinolfson and Van Hoven, 1984). The onset of most flares occurs over a time period on the order of the Alfvén time scale in the corona, but the time scale of the tearing mode is much slower, being a combination of the Alfvén time scale and the much slower resistive time scale. The actual growth rate depends on the wavelength of the perturbation.

For a simple current sheet the growth rate is zero if the wave number k is such that $kl > 1$, where l is the width of the sheet. This means that a current sheet which is shorter than 2π times its width is stable to tearing. For $L_u^{1/4} kl < 1$, small perturbations grow exponentially on a time scale of

$$\tau_{tm} = (kl)^{2/5} L_u^{3/5} \tag{5.26}$$

where τ_{tm} is the growth period of the tearing mode and L_u is the Lundquist number based on the current sheet thickness and the external Alfvén speed. The fastest growing mode occurs when $kl \approx L_u^{-1/4}$ and the corresponding growth rate time scale is $L_u^{1/2}$. For values of kl less than $L_u^{-1/4}$, this expression is not valid.

The threshold condition $kl < 1$ for tearing is a consequence of the fact that the field lines of the initial current sheet resist being bent. An initial perturbation which has a relatively short wavelength tends to straighten out before significant reconnection can occur but, as the wavelength of the perturbation increases, there is more time for diffusion to act. This diffusion occurs in a thin layer in the center of the sheet having a thickness of order $L_u^{-2/5} l$ for the shortest wavelength mode and $L_u^{-1/4} l$ for the fastest growing mode.

The growth and stability of the tearing mode can be affected by many factors, such as the geometry of the sheet, line-tying, the presence of a guide field (a magnetic field component in the direction of the current), externally driven flows, the mechanisms of magnetic diffusivity, and so on. A discussion of such effects can be found in Galeev (1979), Priest and Forbes (2000), and Wesson (1987).

Although a large body of literature is devoted to 2D reconnection, there are still some fundamental questions that remain unanswered. For example, what is the rate of reconnection in a rapidly driven system where the current sheet grows at a rate of the order of the ambient Alfvén speed? This situation occurs in large coronal mass ejections whose speed typically exceeds the local Alfvén wave speed. Also, the effects of strong radiation, thermal conduction, and partial ionization have been only partially explored.

5.4 Reconnection in three dimensions

The addition of a third dimension introduces new reconnection properties and behaviors that are fundamentally different from those in two dimensions. Perhaps the most significant of these is that reconnection can occur in configurations where all field lines have the same topology. That is, the mappings of all field lines of the system are topologically identical. In such configuration the concept of a moving field line becomes ambiguous (Priest *et al.*, 2003).

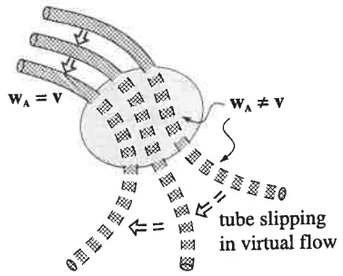

Fig. 5.9. Schematic diagram of the ambiguity that occurs in the definition of field line velocity in three dimensions. The wide broken lines indicate the projection of magnetic flux tubes onto the two-dimensional plane (from Priest *et al.*, 2003).

Figure 5.9 illustrates the situation. Here it is supposed that an ideal conductor, having zero electrical resistivity, surrounds a non-ideal region where reconnection occurs. We suppose for simplicity that there is no fluid flow in the ideal region. Because of the reconnection occurring within the non-ideal region, the mapping of the field lines from their entry point to their exit point changes with time. In three dimensions the change in the connectivity of the field lines can occur in a distributed way, so that any given field line is continually slipping, changing its point of connection to the boundary. Consequently, if one makes a movie of the field line motion by tracing out the field lines at their incoming boundary point, these field lines will appear to move not only within the non-ideal region, but also within the ideal region lying beyond the other side of the non-ideal region. This "virtual" motion in the ideal region occurs even though the fluid in the exterior region is at rest. Thus the virtual motion contradicts the normal requirement that the field lines in a stationary ideal conductor should be at rest. This duality in the definition of the field line velocity is also evident if one simply considers using the exit point of the field line, rather than its entrance point, to trace out the field lines. In this case the field lines on the outgoing side will appear to be at rest while the field lines on the incoming side will appear to move (Priest *et al.*, 2003). Such behavior cannot occur in two dimensions.

5.4.1 *Definitions revisited*

In two dimensions, linear null points fall into two types, namely X-points and O-points, where the neighboring magnetic field lines have X-type or O-type topology, respectively (see the previous chapter). The notion of magnetic reconnection is then fairly straightforward. Reconnection occurs at an X-point, where two pairs of separatrices meet; during the process of reconnection pairs of magnetic field

lines are advected towards the X-point, where they are disconnected and then reconnected. The mapping of magnetic field lines from one boundary to another is discontinuous and, therefore, during the process of reconnection there is a sudden change in the magnetic connectivity of plasma elements owing to the presence of a localized diffusion region where ideal MHD breaks down.

These features of two-dimensional reconnection carry over into three dimensions, provided that there is a well-defined topology. Such a topology will exist if there are appropriate null-point pairs or localized point sources on the boundary (see Chapter 4). However, in many cases of interest an exact topology does not exist. This is especially the case in the solar corona, where reconnection is thought often to occur when null points are not present (Démoulin *et al.*, 1997). To cope with such situations, Schindler *et al.* (1988) proposed that the definition of reconnection should be extended to include all effects of local non-idealness that generate a component ($E_{||}$) of the electric field along a magnetic field. In other words if a localized region exists where

$$\int E_{||}\, \mathrm{d}s \neq 0 \tag{5.27}$$

then reconnection is occurring. Some authors (see Priest and Forbes, 2000) have argued that such a definition is too general, since it includes examples of magnetic diffusion or slippage (such as in double layers or shock waves) that have not been traditionally included in the concept of reconnection.

If nevertheless, we accept the idea that reconnection occurs whenever there is an electric field parallel to the magnetic field then the question arises of how the rate of reconnection is to be defined. In the two-dimensional example of Section 5.3.1, the rate is given by the electric field at the X-line. In the absence of an exact topology and in the presence of a distributed parallel electric field, it is no longer obvious how one should define the rate. However, for the three-dimensional example of Fig. 5.10, such a rate must exist since there is a definite value of flux that is changing its connectivity as a function of time. Hesse *et al.* (2005) showed that the reconnection rate, i.e. the rate at which magnetic flux is newly connected, is given by the maximum value of the electric potential obtained by integrating the parallel electric field along the magnetic field line.

5.4.2 *Reconnection in fields without distinct topological mappings*

In this section we provide a kinematic example of how the generalized definition of reconnection can be applied to a three-dimensional configuration that has no exact topology. (The term "kinematic" refers to the fact that the model does not incorporate the continuity, momentum, and energy equations as would an MHD

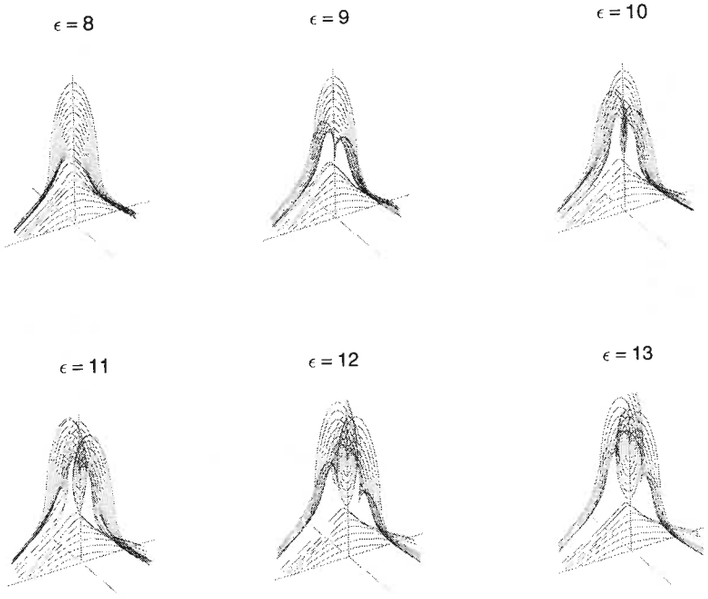

Fig. 5.10. Evolution of the magnetic field in the Hesse *et al.* (2005) model for line-tied reconnection in the corona.

model.) The magnetic field model for this example is (from Hesse *et al.*, 2005)

$$B_x = -1 - \epsilon \frac{1-(y/L_y)^2}{1+(y/L_y)^2} \frac{1}{1+(z/L_z)^2}, \tag{5.28}$$

$$B_y = \frac{1}{4}x, \tag{5.29}$$

$$B_z = \frac{1}{5}. \tag{5.30}$$

Here L_y and L_z are arbitrary scale lengths, which are both set to 5 in the model. This magnetic field does not vanish anywhere, and therefore it does not have the separatrix surfaces or separator line that would exist if null points were present. The effects of reconnection on the magnetic field are simulated by varying the parameter ϵ which determines the amount of flux that has been reconnected at a given time. Figure 5.10 displays an overview of the magnetic field structure for different values of ϵ. The starting value was $\epsilon = 0$, which corresponds to a sheared magnetic arcade. Increasing ϵ leads to the formation of a flux rope that lies above the initial arcade.

From Faraday's equation (Eq. 10.9) we can calculate the inductive electric field associated with the changing magnetic field of the model. By integrating the component of this field parallel to the magnetic field, we obtain the electric potential shown in Fig. 5.11. This potential is not necessarily the total potential; it represents

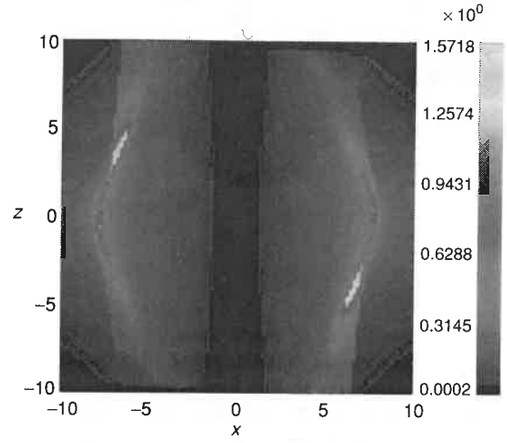

Fig. 5.11. Mapping onto the $z = 0$ surface of the net electric potential produced by induction in the Hesse *et al.* (2005) model for $\epsilon = 10$ in Eq. (5.28).

only the potential caused by the motion of the magnetic field. For this reason it is sometimes referred to as a pseudo-potential (see Hesse *et al.*, 2005). The resulting distribution of the potential on the surface is reminiscent of the chromospheric ribbons produced by solar flares in decaying active regions where the geometry of the magnetic field is similar to that used in the model. At any given time the rate of reconnection is given by the peak value of the inductive potential.

5.4.3 Numerical simulations of three-dimensional reconnection

A large number of fully three-dimensional (3D) MHD simulations have been carried out in which reconnection occurs. However, in many of these simulations the focus has been not on the reconnection process itself but on some other phenomenon or structure in which reconnection plays an important, but perhaps secondary, role. In the last few years there has been an increasing interest in determining the exact nature of the reconnection process occurring in these simulations and in carrying out new simulations specifically designed to determine the nature of 3D reconnection. Figure 5.12 shows the magnetic configuration that occurs in a global simulation of the interaction between the solar wind and the terrestrial magnetic field (Dorelli *et al.*, 2007) for a southward orientation of the interplanetary magnetic field. For a northward magnetic field, the magnetic topology is relatively simple, consisting of a two magnetic nulls with a single separator line between them. However, for the southward case shown in the figure, a more complex situation occurs with many nulls (indicated by the small spheres) and many separator lines connecting these nulls.

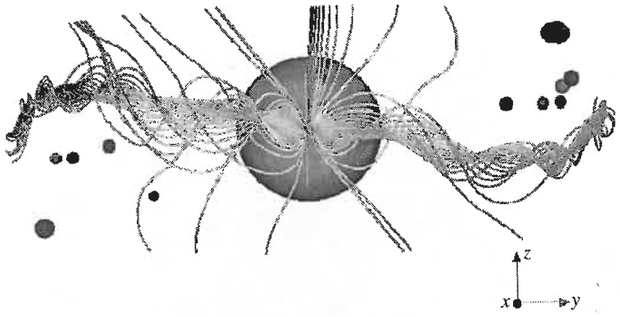

Fig. 5.12. Global MHD modeling of Earth's magnetosphere. This figure shows a view from the Sun of the dayside magnetopause from a global MHD simulation of the terrestrial magnetosphere. In this figure the interplanetary magnetic field is oriented southward, and there is a long flux rope at the sub-solar region of the magnetopause. The small spheres show the location of the multiple neutral points that form. (Courtesy of J. Dorelli.)

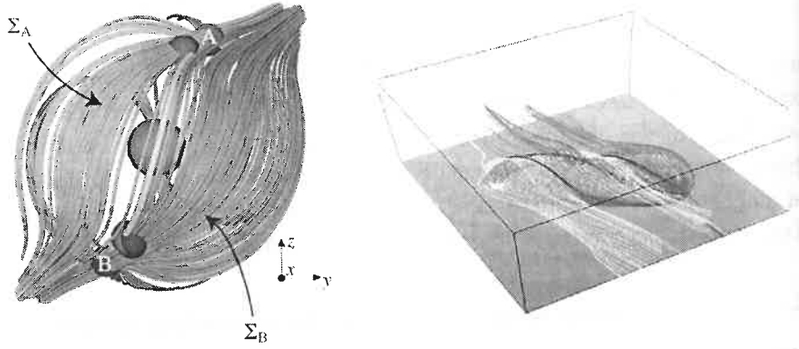

Fig. 5.13. Magnetohydrodynamic simulations of separator reconnection. (Left) A view from the Sun of the Earth's dayside magnetopause for a purely northward IMF, with the Earth's dipole tilted in the GSE yz-plane by 45° (compare with the bottom panel in Fig. 4.3 showing a potential field model in the case where the Earth's dipole field is aligned with the z-axis). A separator line (see Fig. 4.2 for the detailed geometry of such a null–null line) extends across the magnetopause and terminates in the polar cusp neutral points that are indicated by the spheres (from Dorelli *et al.*, 2007). (Right) A simulated solar coronal magnetic skeleton. Two separatrix surfaces intersect to form three separator lines (from Maclean *et al.*, 2006; Hayes *et al.*, 2007).

Idealized simulations are sometimes carried out in order to understand better the complex interactions that occur in more realistic global simulations. Figure 5.13 shows two examples of what is known as separator-type reconnection (Priest and Forbes, 2000). This type of reconnection is common to both the terrestrial magnetosphere (left-hand panel) and the solar corona (right-hand panel). The example in

the left-hand panel is an idealized version of the reconnection process in the Earth's magnetosphere (Dorelli *et al.*, 2007), while the example in the right-hand panel is an idealized version of the reconnection process in compact (i.e. non-eruptive) solar flares (Maclean *et al.*, 2006). The topologies of the magnetic fields shown in both cases are complicated and inherently three dimensional, but many aspects of this 3D complexity are common to both situations.

Three-dimensional numerical simulations have also been carried out to test various 3D analytical models. An example of this type of simulation is the one carried out by Heerikhuisen and Craig (2004) to test a 3D analytical solution obtained by Craig *et al.* (1995). This was is an exact analytical solution of the incompressible resistive MHD equations, and it is closely related to the stagnation-point-flow (Sonnerup and Priest, 1975) and flux-pile-up solutions (Priest and Forbes, 2000) mentioned earlier in this chapter. There has been considerable discussion over the last 30 years about the physical significance of these types of solution. Because the mathematical expression for the reconnection rate in these solutions is independent of the electrical conductivity of the plasma, some authors (e.g. Sonnerup and Priest, 1975) have argued that they correspond to fast reconnection. Other authors (Litvinenko *et al.*, 1996), however, argued that these solutions correspond to very slow reconnection because of the assumption of incompressibility. The numerical simulations have shown that the latter conclusion is correct. Nevertheless, reconnection of this type has been observed to occur in global MHD simulations of the magnetosphere when the interplanetary magnetic field is northward (see Dorelli *et al.*, 2007).

Finally, several 3D numerical simulations have been carried out in conjunction with laboratory experiments specifically designed to study the kinetic aspect of the reconnection process. A recent review of these experiments was given by Yamada (2007).

5.5 Topics for future research

Many aspects of magnetic reconnection have yet to be explored. Even long-studied topics such as steady-state two-dimensional reconnection are not fully understood. Many questions remain about how time-dependent reconnection works in impulsively driven phenomena such as solar flares and geomagnetic substorms. For example, during the impulsive phase of eruptive solar flares the current sheet where reconnection occurs can grows at a rate that exceeds the Alfvén time scale of the system. This rapid growth means that no steady-state reconnection theory applies during the impulsive phase, and there are virtually no theories that predict how the reconnection rate scales with the plasma resistivity in such a situation.

Despite growing evidence that the reconnection process in both solar flares and the terrestrial magnetosphere may be turbulent (McKenzie, 2000; Nakamura *et al.*, 2002), only a few studies have addressed the issue of turbulent reconnection (e.g. Ichimaru, 1975; Lazarian and Vishniac, 1999). The occurrence of plasma turbulence in a highly structure environment poses a severe challenge to large-scale numerical simulations, so progress in this area may be slow for some time to come.

As we emphasized in the early part of this chapter, it seems likely that kinetic effects play an important role in determining how reconnection works both in the terrestrial magnetosphere and in the solar corona. The low rate of particle collisions in the magnetosphere and the super-Dreicer electric fields that are generated in the corona rule out any models that use transport coefficients derived from standard collisional theory. The fact that collisional effects are important does not, in general, rule out the application of MHD theory and simulations in either environment. As Parker (1996) pointed out, ideal MHD theory does not require the plasma to be collisional; it only requires that the electric field in the rest frame of the plasma be small compared with the convective electric field. The principal limitation of ideal MHD theory, insofar as reconnection is concerned, is that reconnection is inherently non-ideal. Thus, some sort of non-ideal treatment is required of the current sheet region where reconnection occurs. In the magnetosphere and the corona this non-idealness requires a consideration of the generalized Ohm's law or its equivalent. The only region where collisional theory is likely to be valid within the current sheet is the solar convection zone, where particle–particle collisions dominate. It seems likely that as numerical simulations of the convection zone become more sophisticated and realistic, interest in how reconnection works in this region will increase.

6

Structures of the magnetic field

MARK B. MOLDWIN, GEORGE L. SISCOE, AND CAROLUS J. SCHRIJVER

6.1 Preamble

One goal this book pursues is to identify phenomena throughout the heliosphere that can be said to be universal. An excellent example of a universal subject is the morphology of magnetically defined structures. The heliosphere is full of distinctive magnetic forms that recur in widely different places. What they are and why this is so are questions we take up here. As a first stab at distinguishing magnetically defined structures, we put them into three groups: current sheets, of which the heliospheric current sheet (HCS) is the largest example; flux tubes, with sunspots as a prototype; and cells, in which we include cavities such as magnetospheres. These three classes make up the common forms of heliophysical magnetic structure that exist on MHD time and distance scales (we are not concerned here with kinetic-scale structures that inhabit the dissipation range of turbulence). Our tasks are to explain why these magnetic structures arise naturally and to describe examples of each. It is important to note that these structures are idealized mental constructs to approximate a real world; we are trying to describe a continuum in black-and-white terms. We should realize that current sheets are not mathematical planes, flux tubes are surrounded by other fields, and cells are leaky in the real world. Nevertheless, these abstractions should help us to think and communicate.

That magnetically defined structures in the heliosphere have been seen to take common forms has led people to recognize over time that there actually exists such a thing as the magnetic organization of cosmic matter (as described, for example, in the NRC report "Plasma physics of the local cosmos", 2001, after which this volume is named). The concept of magnetically organized matter helps to define heliophysics as a unique field of study (cf. Section 1.2) of interesting plasma phenomena in the universe. Parker's monumental *Cosmical Magnetic Fields* (1979) paints a picture of space constantly animated by magnetic field born deep in the convection layer of the Sun, pursuing necessarily a life of turbulent, sometimes violent